Spring 5-11-2023

Determining the Refractive Index of Phytoplankton via Direct Measurement of Cellular Structures

Michael Kamowski

Determining the Refractive Index of Phytoplankton via Direct Measurement of Cellular Structures

by

Michael Kamowski

A Thesis
Submitted to the Graduate School,
the College of Arts and Sciences
and the School of Ocean Science and Engineering
at The University of Southern Mississippi
in Partial Fulfillment of the Requirements
for the Degree of Master of Science

Approved by:

Dr. Xiaodong Zhang, Committee Chair
Dr. Kristina Mojica
Dr. Christopher Hayes

May 2023

ABSTRACT

The refractive index of phytoplankton has never been directly measured before despite its importance towards studying the optical characteristics of marine particles. Previous attempts to measure it have been done through indirect methods. While these methods have proven useful, they contain assumptions about the particles morphology and composition that cause for uncertainty with the measurements. Through the use of the 3D Cell Explorer, a high precision holotomographic microscope, the RI of phytoplankton can be directly measured for the first time. With volume measurements, the phytoplankton were found to not display a single bulk RI, instead the bulk RI was different for distinct groups, largely differentiated by external membrane (Diatoms, Coccolithophores, Dinoflagellates, and Ciliates). Additionally, differences between species were seen in the volume portions of different structures, further necessitating the use of different bulk RIs for different species of phytoplankton. The bulk RI for diatoms shows strong agreement with previous data, validating this method as a way to directly measure the RI of phytoplankton moving forward.

ACKNOWLEDGMENTS

I would like to give acknowledgements to the people who helped make this project possible. Firstly to Drs. Xiaodong Zhang, Kristina Mojica, and Christopher Hayes who each offered expert guidance during many steps of this project along the way and without whom, this project would never have been completed.

I would also like to extend deep gratitude towards my father, Mike Kamowski, as well as Noah and Charlie, all of whom helped me push through the biggest and most stressful points while offering assistance along the way, helping me to keep pushing forward when progress felt most difficult.

Lastly, I would like to extend my warmest thanks to all of my colleagues who assisted along the way through either data collection or helping me to working through problems as they came up.

DEDICATION

I would like to dedicate this Thesis to my late mother, Cheryl Kamowski, who always pushed me to be the best I could, especially when it came to pursuing my passions. Without her, my love for the ocean and all its inhabitants would pale in comparison to what it is today, and for that I am sincerely thankful.

TABLE OF CONTENTS

ABSTRACT ii

ACKNOWLEDGMENTS iii

DEDICATION iv

LIST OF TABLES vii

LIST OF ILLUSTRATIONS viii

CHAPTER I Background 1

CHAPTER II Materials and Methods 7

2.1 Microscope Methodology 7

2.2 Calibration: Filtered Sea Water Medium 9

2.3 Calibration: GLY:H_20 Medium 10

2.4 NASA Exports and Pre-PACE Experiments 11

2.5 Culturing *E. huxleyi* Coccolithophores 14

CHAPTER III Results 17

3.1 Particles Measured 17

3.2 Refractive Index Measurements 20

3.3 Volume Measurements and Weighted RI 22

CHAPTER IV Discussion 25

4.1 Comparison with previous results 25

4.2 Application 27

4.3 Phytoplankton Geometry 28

4.4 Volume Fraction 29

4.5 Ending Remarks 31

CHAPTER V References 33

LIST OF TABLES

Table 1 Volume Portions and RI for different structures of phytoplankton species 23

Table 2 Bulk RI Values for Different Marine Particle Types..... 24

Table 3 Previously measured bulk RI's .....**Error! Bookmark not defined.**26

Table 4 Equivalent Sphere Diameters for 4 phytoplankton..... 26

Table 5 Range of volume portions of measured structures..... 30

LIST OF ILLUSTRATIONS

Figure 1 Diagram of 3D Cell Explorer Microscope 7

Figure 2 GUI of STEVE for Microscope Data Aquisition 8

Figure 3 Calibration Curve for Filtered Seawater.....**Error! Bookmark not defined.**

Figure 4 Calibration Curve for Glycerol:Water Medium 10

Figure 5 Comparison between Filtered Seawater and Glycrol:Water Measurements 11

Figure 6 Sampling Stations during Pre-PACE Cruise 12

Figure 7 *E. huxleyi* population Growth Curves 15

Figure 8 Sidescatter Measurements of Treated and Control *E. huxleyi* Populations..... 16

Figure 9 Various Diatoms Sampled During Cruises..... 17

Figure 10 Various Non-Diatoms Sampled During Cruises 19

Figure 11 Refractive Index Measurements of External Membranes 20

Figure 12 Refractive Index Measurements of Internal Components 21

Figure 13 Volume Measurements of Various Phytoplankton..... 30

CHAPTER I Background

The refractive index (RI) is an optical property of a material describing how light interacts with it. RI is a measure of how the speed of light changes in passing from one material into another, relating it closely to the density of the medium (Matthew 1916), which in turn is determined via composition. The RI is represented by a complex number of the form (n=n'+ik) with n' representing the real portion of the RI, responsible for scattering processes, while k represents the imaginary portion of the RI, and dictates the absorption properties of the medium. These two processes, scattering specifically, are also affected by the particles size, shape, and structure, but the driving force behind these interactions is this RI. Therefore, knowledge of the RI of particles will not only provide information regarding particles composition and density, but also how incident light interacts with these particles by way of scattering and absorption.

Despite the importance of RI, measuring it directly for application towards microscopic particles is particularly challenging, largely due to particle size (<200μm) being too small for traditional methods to be effective. Consequently, various indirect methods which rely on measuring alternative properties (ex: scattering) and relating them back to the RI are used. One commonly used approach, Immersion Refractometry, estimates the RI of particles through suspension in various media of differing RI values (Faick et al. 1944). The driving principle behind this method is that when the particles external membranes and the medium have the same RI, they will scatter light identically, causing the membrane to become invisible. This method, however, will only provide measurements for the external membrane. Phase Contrast Microscopy (Zernike 1942) operates along the similar principles with the improvement of allowing a more detailed

look within the particle. Flow Cytometry uses a combination of scattering and fluorescence measurements along with modeling to determine the complex RI of microscopic particles (Ackelson et al, 1988; Ackelson and Spinrad. 1988; Spinrad and Brown, 1986). Comparing the measured absorption and attenuation efficiencies to modeled spectral values of populations of particles can also be used to measure RI (Bricaud et al. 1988). RI can also be measured through the scattering measurements collected at one angle (Zaneveld et al. 1974) Further studies have shown use of the Volume Scattering Function (VSF) which describes the angular distribution of light scattered by a particle, along with attenuation measurements to determine RI (Twardowski et al. 2001; Zhang et al. 2011). There has also been a method developed that uses the incident angle of light and polarization along with a Muller Matrix inversion to calculate RI (Fan et al. 2017). With many of these methods, the results are compared with Mie theory to determine validity of the results. Mie theory models the theoretical scattering of an electromagnetic wave when it interacts with a homogenous and spherical particle (Mie 1908). Being able to model the scattering of particles by changing various properties, such as size and/or RI is invaluable towards the continual development of methods for measuring these particles.

While these methods are useful, they do have their own inherent uncertainties due to their assumptions about the particles they are examining. One of the biggest assumptions is that these particles are all homogenous throughout, which results in a single RI to represent the particles in bulk. Immersion refractometry and phase contrast microscopy do not have this assumption however, they are unable to. Furthermore, when Mie Theory is applied with these methods, the particles themselves are assumed to be spheres.

However, natural marine particles are seldom spherical or homogenous. Green et al (2003) found that to accurately model marine organisms, one must characterize how they differ from these homogenous spheres to account for the changes due to this mixed composition itself. Zaneveld (1974) proposed that the optical properties of a particle do not average in a linear fashion, showing the necessity of a more complete understanding of the RI distribution within a particle. Instead, these particles are more accurately represented as a collection of multiple homogenous spheres with differing refractive indices. Others have also attempted to resolve this issue through the use of coated heterogenous spheres (Organelli et al. 2018; Poullin et al. 2018) to remarkable success, which is detailed later. Ultimately, the homogenous and spherical assumptions that are used by these methods are unrealistic and result in significant uncertainty associated with the derived values for refractive indices of these particles.

There has been one significant attempt at describing the bulk RI of phytoplankton particles through examining their metabolite composition (Aas 1996). He collected and combined all available RI data on the metabolite compositions of various different phytoplankton. He also demonstrated that the water content of a phytoplankton and its RI have a strong correlation when cells have a water content of 50% or higher. The dry mass of each phytoplankton species was divided into four categories: proteins, carbohydrates, lipids, and pigments. He further classified the outer shell of specific planktonic groups as: coccolithophores with calcium carbonate and diatoms with silica. Next, he found the refractive indices for each of these cellular components and obtained a bulk RI for the dry mass of the phytoplankton by weighting each component by its mass fraction. With the dry portion accounted for, all that was left was the water portion, however, as

phytoplankton are mostly water by volume (upwards of 80%), this water is the source of a lot of uncertainty in measuring the RI. Using previously available data describing the water content of phytoplankton ranging between 60%-80%, Aas used the Lorenz-Lorentz Equation to calculate the mean RI for different phytoplankton taxa based on the dry mass and a variable water content. The results showed that although the RI does differ among phytoplankton species; the variance was small. For example, with a 60% water content, the biggest difference in RI of 0.010 was seen for Coccolithophores and Brown algae (1.424 – 1.414, Coccolithophore and Brown Algae respectively), and with an 80% water content, this difference shrinks down to 0.005 (1.381-1.376). In general, as the water content increased, the bulk RI decreased towards 1.339, approaching the average RI of seawater. Moreover, the bulk RI of a particle varied due to differences in the density of the particle, i.e., less dense particles (that is, a higher water content per unit volume) had a lower bulk RI compared to higher density particles. Furthermore, he posited that the higher density particles were primarily inorganic in nature while the lower density particles were more representative of organic particles and phytoplankton as a whole.

Three different factors were not considered by Aas that would alter the RI measurements of these phytoplankton. First, some phytoplankton have been observed as clumping together or becoming embedded with inorganic particles, specifically mentioning metal oxides which can account for a small percentage (1-4%) by dry mass of various diatoms. However, this was not something Aas accounted for in his measurements, choosing to ignore the potential inclusion of these metal oxides due to the small effect they would have. The second consideration is that structure, both internal and external as well as differences between species were not considered. That is, it was

assumed that particles were uniform in both shape and internal composition. Additionally, in my examination of dinoflagellates in particular, the external membrane measurements have a higher amount of uncertainty due to the biology of these organism, they can take on one of two different types: armored and unarmored. The armored versions are noted for having an external structure consisting of interlocking plates, called the theca, composed of mostly cellulose. The unarmored forms of dinoflagellates do not have this structure and subsequently have a different RI for their external membranes which is where the uncertainty lies. The third issue is that the bulk RIs were calculated indirectly from the various composition, not through direct measurement. In assuming the values from literature, the measured values could be different due to differences both structurally as well as chemically in their composition. In my examination, my measurements were similar but ultimately not the exact same as what Aas compared to in his study. While his results on the RI of phytoplankton have been widely cited (245+ citations), there has not been any meaningful attempts to verify these results through direct measurement.

The 3D Cell Explorer by Nanolive is a high precision tomographic microscope that generates a 3D image of a sample with contrast dictated through differences in refractive index. It allows a user to examine both the external and internal structure of particles as small as 10μm in a very quick and cost effective manner. With this instrument, I am able to examine phytoplankton cells and directly measure the RI of various portions of the organism. When measuring these particles, even precise measurements on the volume of different structures can be collected as well. The goal of this study is to directly determine the bulk RI of marine organisms. With this, I designed my hypothesis as such:

- **Hypothesis**
    - One bulk RI cannot be used to describe all phytoplankton due to differences in composition and structure

CHAPTER II Materials and Methods

2.1 Microscope Methodology

The 3D Cell Explorer utilizes a rotational interferometric technique to map a particle as a holographic image that is constructed from the measured refractive indices of different cellular components (Fig. 1a). The instrument shines a laser, which is subsequently split into two beams (Fig. 1b). The first beam travels unimpeded and is called the reference beam. The second beam is directed towards the sample and is called the sample beam. When the sample beam passes through the sample, it is altered and creates an interference pattern due to its interaction with the particle. These two beams then come together, and their interference is recorded (via a software called STEVE). Once this happens the laser rotates by a small angle and repeats this process until it

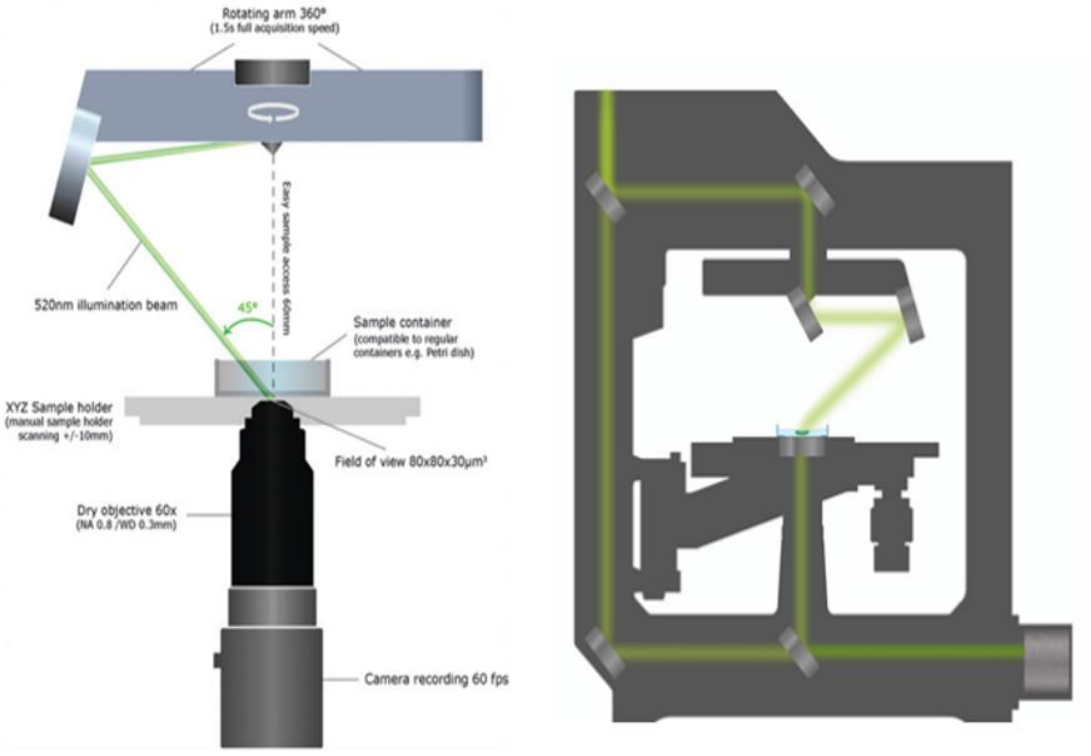

Figure 1 *A) Path of the incident beam for sample illumination in the 3D Cell Explorer. The top arm rotates to collect from every angle. B) Diagram showing the optical path of the beam of light detailing how it is split and later recombined.*

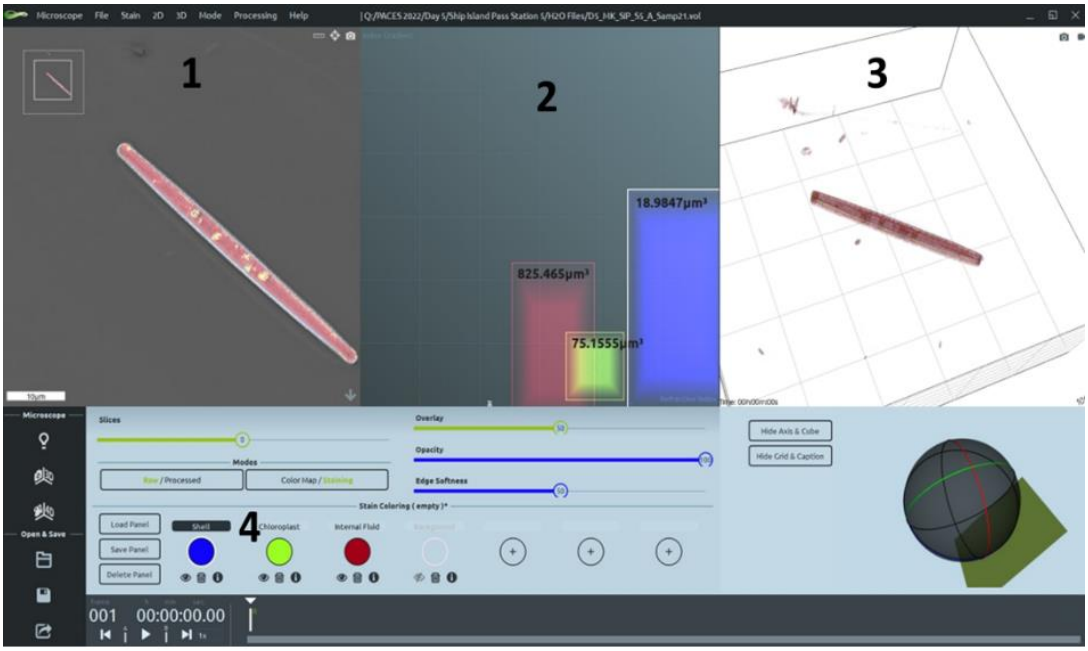

Figure 2 *GUI of STEVE Program for data acquisition from 3D Cell Explorer Microscope. 1) Sample Image 2) Stain Field 3) 3D Reconstruction of the sample based on RI measurements 4) Stain painter where colors are chosen for measuring RI and Volume.*

collects a 360 degree view of the sample. After one 360 degree view, the STEVE program then collects and combines the separate interference "images" collected at each angle and forms a 3D holographic image. In addition to this rotational technique, the microscope utilizes a specially designed "high-numerical-aperture", meaning that instead of collecting light at one aperture like typical microscopes, it actually collects it at many small apertures. This design is what allows the microscope to collect images that are of the particles with resolution up to twice what is traditionally possible (Pollaro et al 2015). The resulting resolution on the RI is ±0.001. The instrument has a total field of view of 80x80x30 µm, allowing direct visualization of particles within this size range. With this 3D Holographic reconstruction, the distribution of the RI of the sample can be viewed from any viewpoint. The STEVE Program allows detailed examination of a particle using digital staining to single out portions of the particle with similar RI values. Figure 2

displays the STEVE program that was used for collecting the distribution of the RI and volume (in terms of μm^3 as well as pixels) that each bin of RI values occupies. The program will then apply a 'stain' to any pixels in the sample that are within the same range of a specific RI. A major advantage of this method is the low cost of operation as well as the precision and speed data can be collected. Furthermore, digital staining allows for the particles to be analyzed without any physical alteration, which results in a lower amount of possible error.

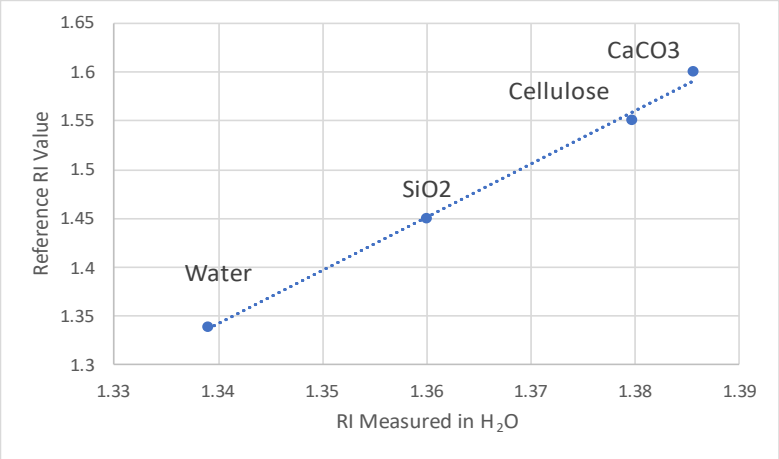

Figure 3 *Calibration curve for particle component analogues measured from within filtered seawater.*

2.2 Calibration: Filtered Sea Water Medium

The 3D Cell Explorer's design provides high precision (0.001) measurements of RI. However, our preliminary analysis revealed that the resolution of RI measurements (i.e., the ability to resolve differences) is directly dependent on the suspension media. That is, the operational range of measurements of the RI of a sample is ± 0.01 of the mediums RI. Therefore, to increase the resolution, the difference between the sample RI and the mediums RI should be similar but not identical. For example, using seawater as the medium (RI = 1.339), the range of the RI that is able to be resolved is 1.239-1.439. For the organelles with Ri outside this range, such as the chloroplast (i.e., RI = 1.47) and some outer membranes estimated between 1.45-1.6, their values would not be able to be resolved.

To resolve this issue, a calibration curve had to be developed. Silicon dioxide, calcium carbonate, and cellulose were measured within a filtered seawater medium. Additionally, the background was measured to serve as a blank. The averages of the measured values were plotted against the reported literature RI values of these samples in figure 3 along with a linear regression. The literature values were obtained from Aas (1996). This regression line allows me to scale the measured values to their reference value in order to correct for when the particles are measured in water. The data itself displays a linear correlation and the subsequent regression gave us the equation: **y = 5.4525x – 5.9639** with an R^2 of 0.9959, showing the data has a strong fit to this regression model.

2.3 Calibration: GLY:H_20 Medium

I also performed a calibration in a mixture of 75% Glycerol:25% DI H_2O with a RI of 1.44 to serve as the medium. The RI of this medium was confirmed using an ABBE Refractometer. The intention for this solution was to determine whether it would give accurate measurements of the cellular structures given that the RI is within the range of the cellular components. With this medium, the range of RI would be 1.34 to 1.54. Average measurements of the RI for

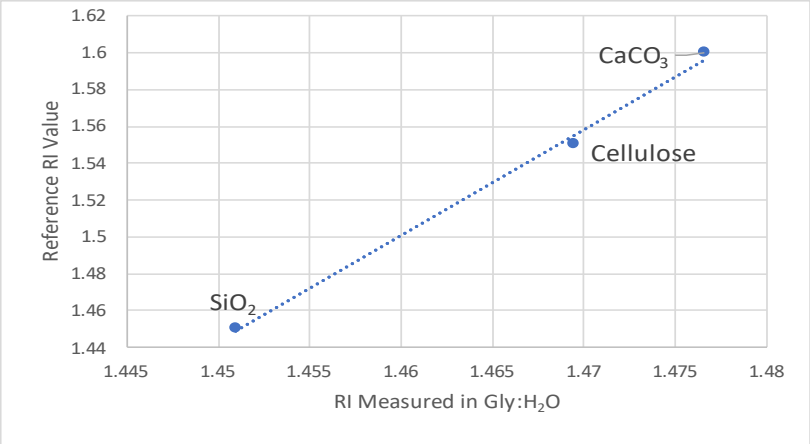

Figure 4 *Calibration curve for particle component analogues measured from within a medium of 75%:25% Gly: H_2O.*

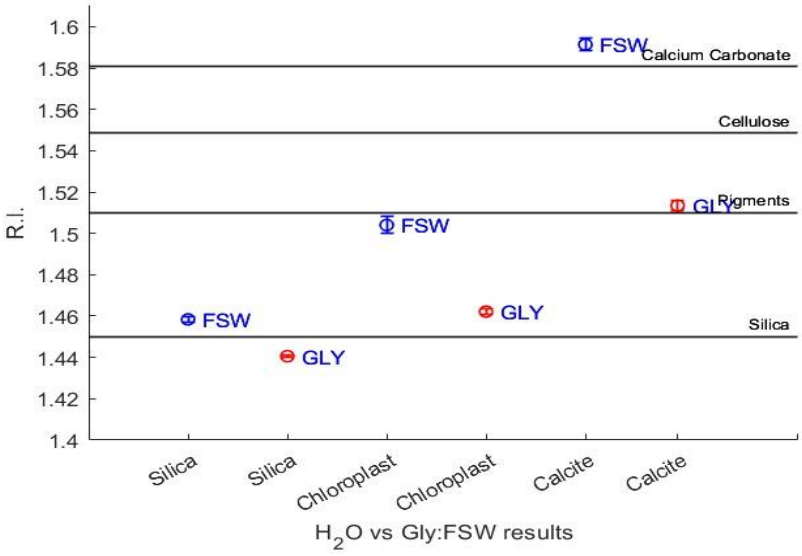

Figure 5 *Comparison of measurements in FSW (Blue) and Gly:FSW (Red). Standards for comparison are displayed as black lines.*

silicon dioxide, calcium carbonate, and cellulose were taken from within this medium and subsequently plotted against reference literature values for these same substances, shown in Figure 4. A linear regression was applied in order to examine the results and its close fit (R^2 = 0.9942) shows its validity in measuring these components as well. However, in comparing the two curves, the Glycerol calibration seems to underestimate the RI compared to the filtered seawater calibration (Fig 5). Additionally, the similar RI between the Glycerol/H_2O medium and the outer walls of diatoms (Silica, n=1.45) decreased resolution to the degree where the external silica structures were no longer resolvable. This issue was particularly prevalent when examining *Chaetoceros spp*. and *Skeletonemia spp.* as these genus' have long thin protrusions off of the cell body as part of their chain linking structure.

2.4 NASA Exports and Pre-PACE Experiments

The first of the experiments occurred during the May 2021 NASA EXPORTS Cruise. My colleague and collaborator for multiple portions of this study, Kacey Lange, was aboard the RRS Discovery as a part of this cruise. The sample locations they visited were

all from within an anticyclonic eddy centered at 50°N, -15°W in the North Atlantic. During this month long cruise, water samples were collected at 2 depths, the top 5m of the water column, and the depth of the Chl-a Max. While the two depths are normally differentiable, during the second half of the cruise a hurricane that passed through the study area which thoroughly mixed the water, removing any stratification present. Following sample collection, the samples were brought to the lab onboard the ship where they were examined under the 3D Cell Explorer. The water samples were concentrated over a 10-20 µm mesh into 10 mL and subsequently examined in 50 µL aliquots for particle identification.

In February of 2022, a joint research cruise between the University of Southern Mississippi, The University of North Dakota, and the Naval Research Laboratory was conducted as part of a pre-PACE experiment. The PACE (Plankton, Aerosol, Cloud, ocean Ecosystem) satellite is a satellite that NASA will be launching in November of 2023. It will function to examine many processes and their impacts on the planktonic

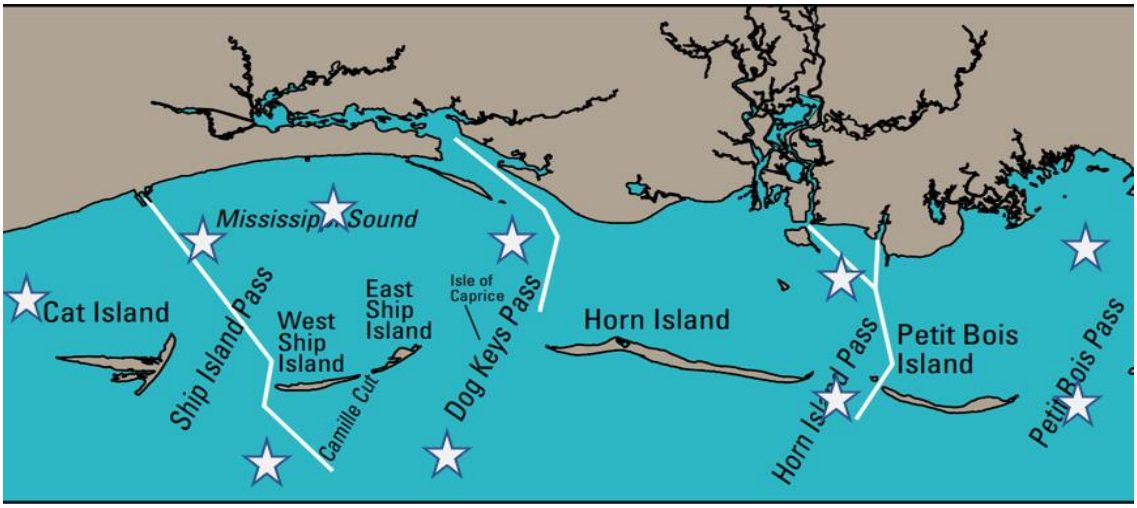

Figure 6 *Map of the Mississippi Gulf Coast showing the barrier islands that were transected between during the PrePACE Cruise in February 2021. Different color pins represent the various transects completed.*

organisms as well as monitor global views of the surface of the ocean. This experiment consisted of multiple cruises, each of which transected between two barrier islands along the Mississippi gulf coast (Fig 6). During the course of this experiment, water samples were collected at various stations. The aim was to collect a wide array of different particles to allow for a more comprehensive analysis of various phytoplankton particles that were present. With phytoplankton being ubiquitous, examining species from different locales is invaluable to our overall understanding of these particles. When arriving back at the lab, 500 mL – 1 L of the sample would be taken and stored within a 4°C fridge overnight before analysis.

To begin analysis, 50-200mL of sample was filtered via Vacuum filtration using 2 µm Nucleopore Tract-etch Membrane from Whatman Lab at minus 0.4-0.2 bar of pressure. The different volumes were dependent on whether the filter was clogging with larger volumes. If the samples did not clog, then 200 mL was filtered, if they did clog then smaller volumes were concentrated in 50 mL increments on the same type of filter. Following this, the samples were rinsed off of the filters and using either filtered seawater or the glycerol medium for analysis under the microscope. In this filtration and concentration step, the samples were concentrated down to 4 mL and stored in a 15 mL centrifuge tube. For data collection, 0.25 mL of each sample was pipetted out onto a microscope slide. A coverslip was subsequently placed onto the slide and the slide was placed under the microscope. Once the slide was in place, the sample was swept through and examined for any particles/organisms of note to collect data for. When a particle/organism was found, the data acquisition via the STEVE program was

performed. With each sample, the microscope was calibrated to the RI of the filtered seawater medium, setting the background RI to be equal to 1.339.

To process the data, each file was loaded into the STEVE program and then digitally stain the external membrane, the chloroplast (if present), the background medium, and the internal fluid of the phytoplankton (if possible). From this, the mean value for the RI of the portion that was stained, along with an approximate volume of the stain itself, were both obtained. With these volume measurements, we are able to estimate the volume-weighted average RI value for the whole particle. I will call this averaged value the bulk RI of the particle.

2.5 Culturing *E. huxleyi* Coccolithophores

Coccolithophores are noted for their distinct external membrane consisting of a series of calcite ($CaCO_3$) scales, called coccoliths. This structure is of ecological and global importance because it plays a key role in carbon cycling of the ocean (Rost 2004). For this study, another importance of these organisms is the ability to cause these coccoliths to be removed, creating “Naked Coccolithophores”, allowing us to view the cellulose membrane underneath them (Walker et al 2018). Ultimately through the removal of these coccoliths, the underlying cellular structure can be examined and measured. Here we decalcified the coccolithophores through the use of HCl to dissolve the coccoliths directly (Santomauro et al. 2016; Haunost et al. 2021). For this experiment, cultures of *E. huxleyi* coccolithophores (Strain CCMP 371) were grown axenically, that is free of outside biological contamination, in an L1-Si/25 media (Guillard & Ryther 1962) which does not contain silica. The cultures were grown inside 25ml culture flasks (Corning Incorporated, 353107) inside a culture chamber (Sanyo Scientific, MLR-351/351H) at 20°C.

These cultures were kept under a 12:12 Day/Night Cycle with media transfers occurring every 2 weeks. During the day part of the cycle, the cultures were exposed to a constant photon flux of 45 µmol/m^2*s (measured with a Quantum Meter from Apogee Instruments). In order to maintain the cultures as axenic, we utilized a Biological Safety Cabinet (Safety Plus, Herasafe 2030i) when the cultures were not in the culture chamber as well as autoclaving any used materials as well as the media prior to use. At the beginning of the experiment, the pH of the media was adjusted to 7.8 (measured with a Mettler Toledo pH meter, EL20-Basic) and was maintained throughout the growth of the cultures.

The cultures were measured throughout the week prior to decalcification to track their growth. Abundance was measured using, a BD FASCelestra BVR flow cytometer excited using the blue 488nm argon laser and the 600LP and 695/40 emissions filters. The signals were distinguished using bivariate plots of SSC and 695/40. Growth measurements were used to distinguish when cultures reached the stationary growth phase. Figure 7 shows the growth curves for each population, clearly showing the stop in growth associated with reaching the stationary phase which was reached at roughly 5*10^5 cells/mL. When the cultures had reached this stage, they

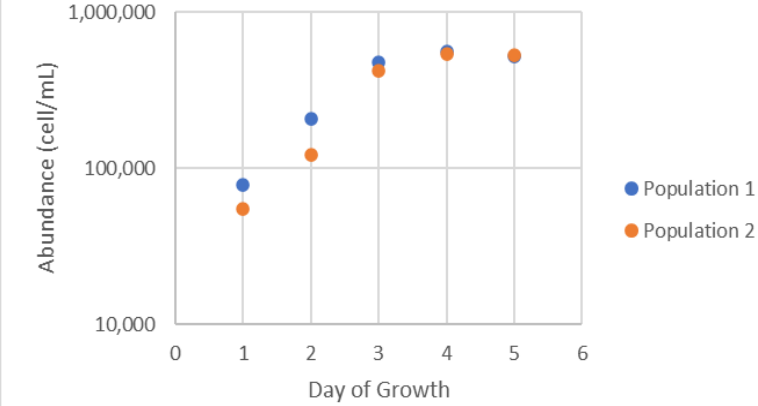

Figure 7 *E. huxleyi population abundances for two populations cultured for 1 week before decalcification. Day three is when the growth begins to flatten out, signifying the start of the stationary phase.*

were then put into a darkness phase where they were kept in the dark within the culture chamber for 36-48 hours. This darkness phase is necessary in order to deplete the phytoplankton of their excess energy, preventing them from rebuilding their coccoliths following acidification. From this step onwards, everything was performed under very low light levels to prevent any unintended effects due to the light itself. To decalcify the coccolithophores, two of the cultures were reacted with 2.5 mL/L 1M Hydrochloric Acid (HCl) in order to dissolve the coccoliths. The flasks were mixed for a minute, during which their pH dropped to 4.8, before using sodium hydroxide (NaOH) to bring them back up to the pre-acidification pH (7.8). Immediately following the neutralization, each sample was measured via FCM to determine cell loss due to this methodology and revealed negligible losses in abundance counts. Figure 8 shows a pair of samples containing a mixture of both acidified and unacidified cells, the different side scatter measurements confirmed the efficacy of this method for removing the coccoliths of the organisms.

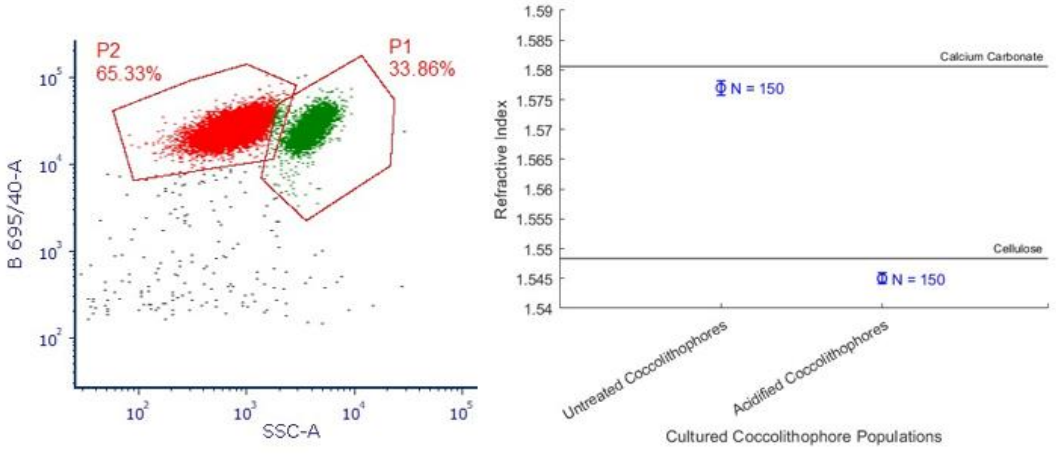

Figure 8 *a) Measured sidescatter for a mixed population consisting of P1: Untreated Coccolithphores and P2: Acidified coccolithophores. The difference in sidescatter is due to the dissolution of the calcite scales. b) Refractive Index measured for the two populations, with the acidified cells displaying lower refractive index due to the loss of calcite.*

CHAPTER III Results

3.1 Particles Measured

Across the two cruises, a number of diverse particles/organisms were sampled and measured, most of which were phytoplankton. Of the phytoplankton, the most abundant organisms were diatoms, specifically members of the genus *Chaetoceros* or

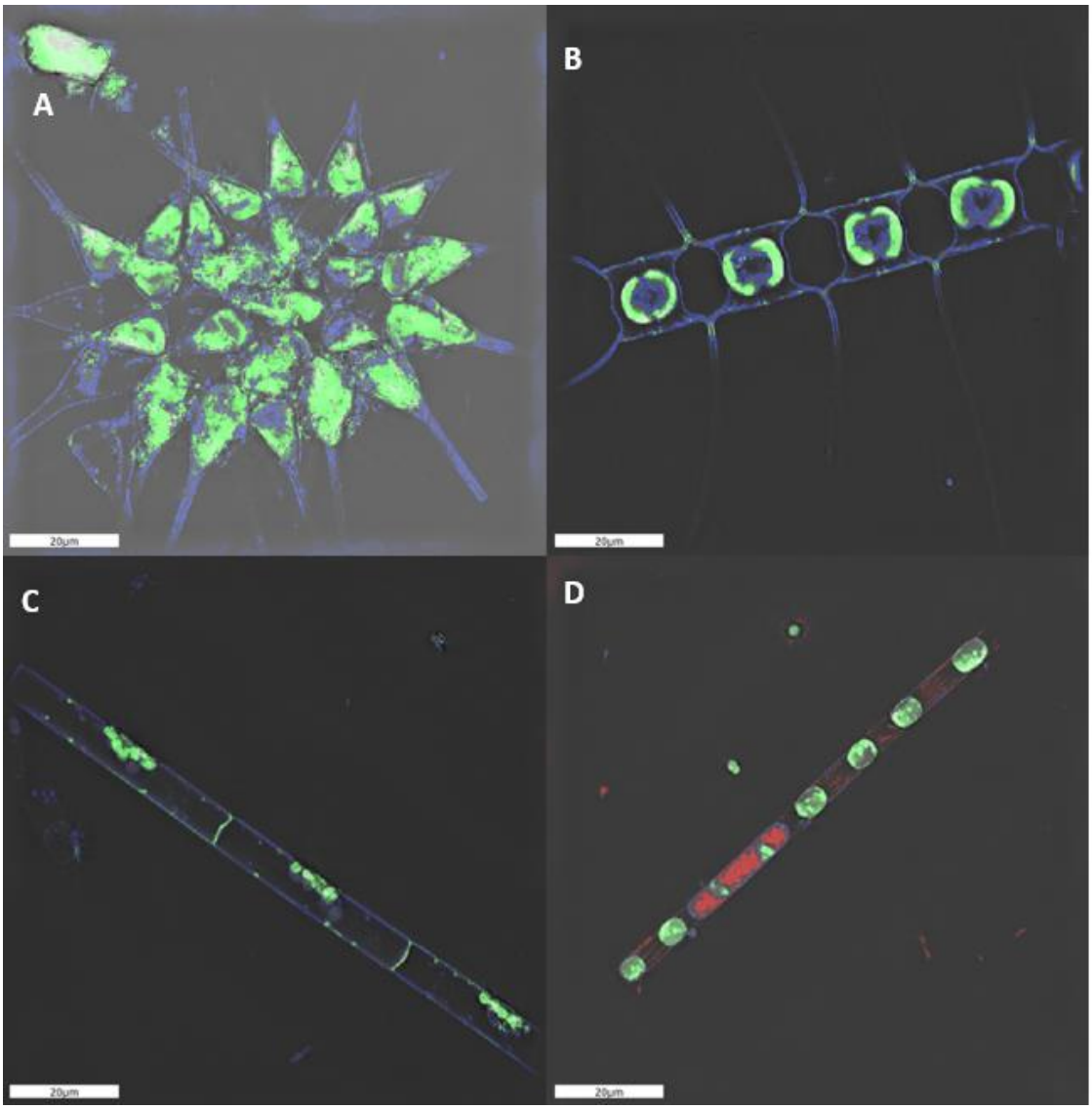

Figure 9 *Measured Diatoms a) Chain of* Asterionellopsis *in girdle view, b) Chain of* Chaetoceros *in broad girdle view, c) Chain of* Guinardia *in broad girdle view, d) Chain of* Skeletonema *in broad girdle view. The different colors correspond to different cellular structures: blue corresponding to the silica membrane, with green representing the chloroplast(s)*

Skeletonemia. Other diatoms that were observed included *Pseudo-Nizschia, Bacteriastrum, Asterionellopsis, Thalassionema,* and *Eucampia*. Aside from diatoms, I also observed and measured Dinoflagellates and Ciliates, two other small marine organisms. In the Pre-PACE cruise, I also collected various marine flocculates consisting of oil particles encased in aggregations of silt or clay particles, formed due to the conditions of the area itself. Figure 9 displays multiple diatoms I encountered and measured while sampling the water. In the figure, the blue portion corresponds to the silica frustule whose measured RI value was 1.458, the green corresponds with the chloroplasts which measured near 1.5, and the red corresponds to internal fluid which measured at 1.35. In comparing these with the measured standards, the measured values agree with the previous measurements by both Aas (1996) and my own.

Figure 10 displays some non-diatom particles that were encountered. These included a (A) a flocculate, (B) a dinoflagellate *Prorocentrum spp.*, (C) a coccolithophore *Emilania huxleyi,* and (D) a marine ciliate. In Fig 10(A), the external membrane of the flocculate measures near 1.35 while the internal portion is much lower, at 1.268. This outer membrane is likely composed of clay particles aggregated together with some clumping agent. The middle region measurement being near the lower bound of the instrument (1.24) supports the possibility of the internal portion being trapped air or oil. Fig 10(B) shows a *Prorocentrum spp.* Dinoflagellate, with the cellulose membrane measuring 1.545. In the image, it is also easy to see the lack of apparent structures visible in the organism making measurements of the chloroplast difficult. For the coccolithophore in Fig 10(C), the blue portion is the cellulose plates, measured at 1.545, while the green chloroplasts measured at 1.504. In Fig 10(D), the blue stain is the

phospholipid membrane of the ciliate which measured at 1.38 while the internal portion measured around 1.52. Due to their small size (5-10 μm) the instrument had difficulty in gaining detailed images of the internal structure of both the coccolithophores as well as the ciliates, so there is likely some effect due to error.

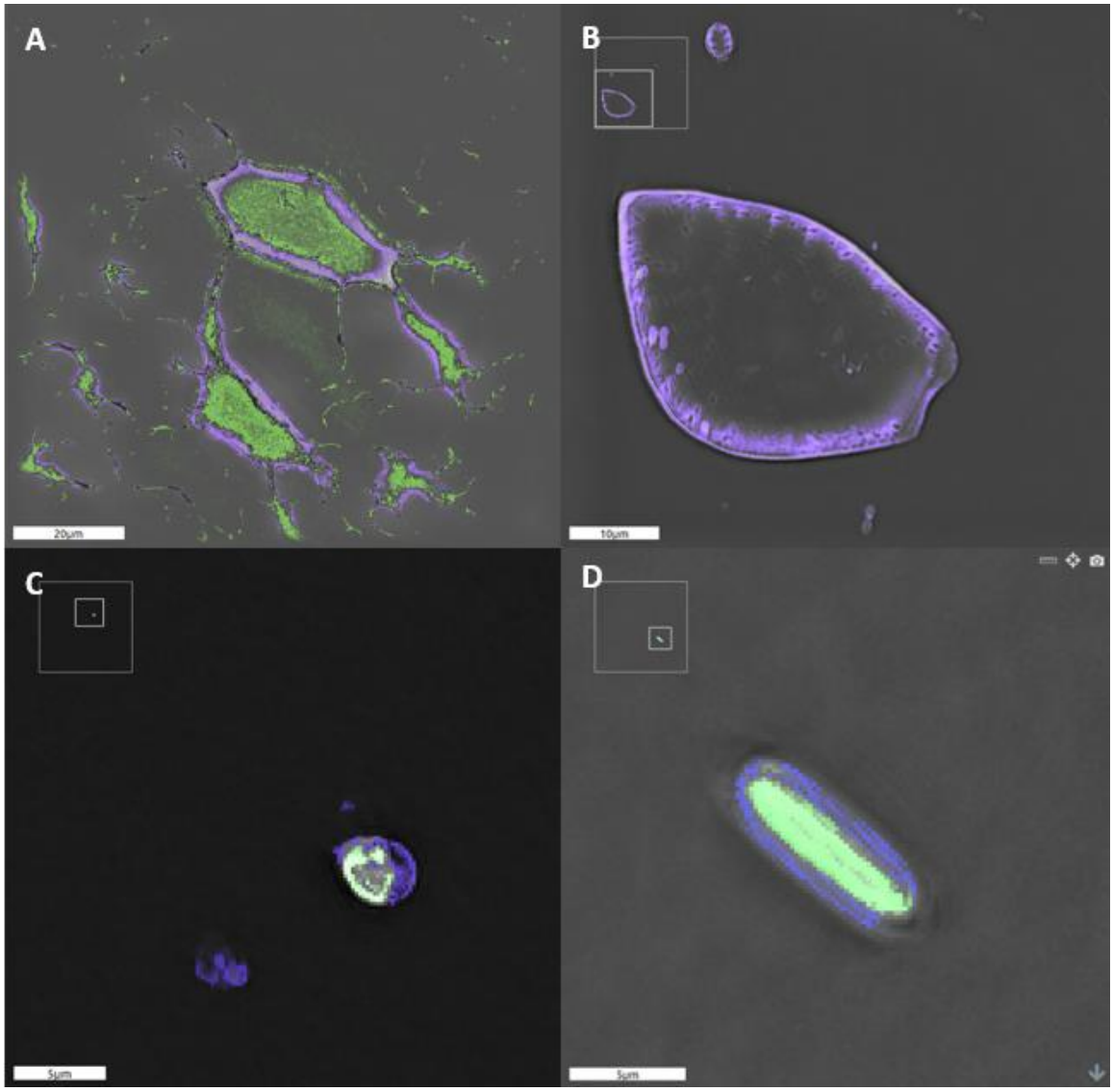

Figure 10 *Other marine particles sampled a) marine flocculate b) dinoflagellate* Prorocentrum spp. *c) coccolithophore* Emilania huxleyi, *d) marine ciliiate. The blue color corresponds to the outer membrane while the green stain corresponds to internal structure, where detectable. In the flocculate, the red corresponds to an internal medium differentiable from the surrounding seawater*

3.2 Refractive Index Measurements

The Nanolive provided membranes of different distinctive RI values for several different types of organisms. Figure 11 shows the values for the RI of the shell of four representative organisms, measured in water: diatoms with a silica frustule, dinoflagellates with a cellulose membrane, coccolithophores with calcium carbonate coccoliths, and ciliates with a phospholipid membrane. Each of the measured structures strongly agrees with the RI of their corresponding standard. The values for these analogues were obtained from Aas (1996). Figure 12 shows the data for the internal portions of these organisms. Like the external membranes, there is a clear differentiation

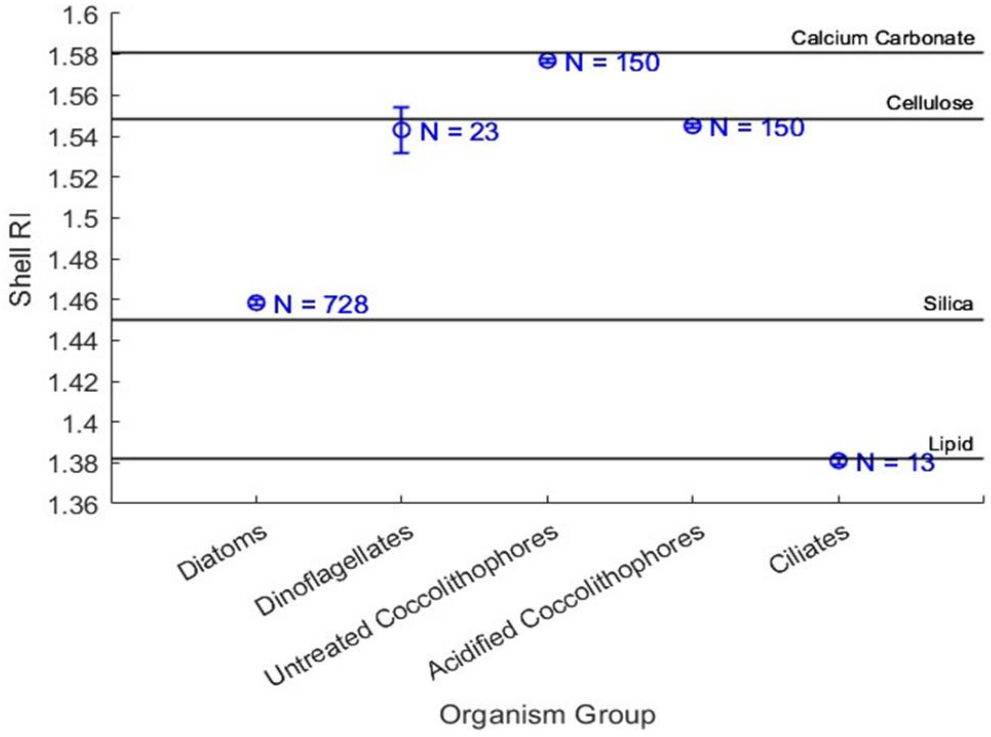

Figure 11 *RI values measured for outer shell membranes of 4 groups: diatoms, dinoflagellates, coccolithophores (both acidified and unacidified), and ciliates. Horizontal black lines represent the RI values of analogues to these membranes from Aas (1996).*

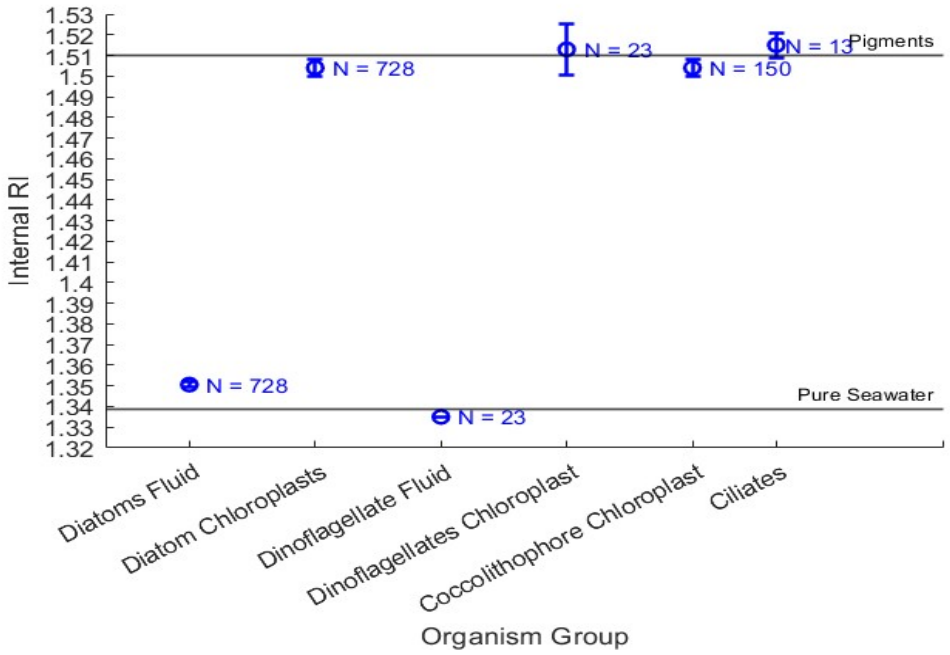

Figure 12 *RI values measured for different internal structures of 4 groups: diatom fluid and chloroplast, dinoflagellate fluid and chloroplast, coccolithophore chloroplast, and ciliate internal structure. Horizontal black lines represent the RI values of analogues to these structures from Aas (1996)*

between the different structures that were measured. The internal fluid of the diatoms and the dinoflagellates, the chloroplasts of the diatoms and coccolithophores, as well as the internal portion of the ciliates were all measured. The reference values for the average RI of photosynthetic pigments, obtained from Aas and for water are represented as black lines (1996). For the dinoflagellates, the internal portion was not easily measurable (Fig 10b), so the values here most likely represent the internal fluid of the organism, the cell sap. This cell sap is similar to seawater; however, it varies in ionic content with different species having different specific concentrations (Kahn 1978; Aas 1996). The mean internal RI values for both dinoflagellates and diatoms are close to that of water, meaning that the internal fluid is likely seawater mixed with intracellular cytoplasm. The higher value seen in the diatoms is likely due to the specific makeup of the internal fluid not being pure seawater. For the chloroplasts and ciliates, the value for the photosynthetic

pigment standard compares very favorably, with the slight variance observed likely due to the specific makeup of the pigments within the different species. The ciliates themselves were small (5-10 µm) which did not allow for high enough resolution to determine any internal structure, seen in Fig 10d. The coccolithophores measured via the 3D Cell Explorer similarly did not display any meaningful internal structure due to their similarly small size (5µm), aside from the presence of a large chloroplast occupying a sizable portion of the internal volume, which is shown in Fig 10c. This is an issue due to the small size of these particles being towards the lower bound of the instruments imaging range (<5 µm). In order to better examine the internal structure, either larger species would need to be measured or cultured.

3.3 Volume Measurements and Weighted RI

With collecting both RI measurements for the various portions (Fig 9 and 10), as well as volume estimations (either direct from the STEVE program itself or indirectly through visual estimations), the overall RI of the particle can be determined through the formula:

$$(1)\ n_{bulk} = \sum_i (n(i) * \frac{V_i}{V_{total}}).$$

This gives us a total weighted RI which should account for the overall interaction caused by the particle itself, i.e., the bulk RI. The estimated bulk RI of various phytoplankton are listed in Table 1. The RI for the different large structures of the phytoplankton are presented along with their relative volumes. Additionally, the bulk RI and whole volume is given along with the approximate partial water volume. As different phytoplankton

Table 1 *Volume Portions and RI for different structures across various phytoplankton species*

Species	Shell	Chloroplast	Water	Weighted RI
Chaetoceros	1.458 ± 0.001	1.504 ± 0.004	1.34	1.375
n = 209	21.58 ± 14.47%	5.56 ± 5.43%	72.86 ± 19.04%	
Pseudo-Nitszchia	1.458 ± 0.001	1.504 ± 0.004	1.34	1.411
n = 53	44.59 ± 21.38%	10.85 ± 7.23%	44.57 ± 24.17%	
Thalassionema	1.458 ± 0.001	1.504 ± 0.004	1.34	1.368
n = 64	18.77 ± 4.31%	3.5 ± 1.93%	77.72 ± 4.87%	
Bacteriastrum	1.458 ± 0.001	1.504 ± 0.004	1.34	1.365
n = 15	11.09 ± 4.3%	7.26 ± 1.71%	81.65 ± 2.73%	
Rhizosolenia	1.458 ± 0.001	1.504 ± 0.004	1.34	1.358
n = 39	8.48 ± 5.14%	4.96 ± 8.17%	86.56 ± 12.46%	
Skeletonema	1.458 ± 0.001	1.504 ± 0.004	1.34	1.364
n = 296	14.97 ± 5.81%	4.09 ± 3.66%	80.94 ± 8.66%	
Cylindrotheca	1.458 ± 0.001	1.504 ± 0.004	1.34	1.399
n = 18	28.45 ± 9.69%	15.46 ± 4.03%	56.08 ± 13.55%	
Eucampia	1.458 ± 0.001	1.504 ± 0.004	1.34	1.356
n = 13	9.52 ± 0.79%	2.93 ± 0.28%	87.55 ± 1.03%	
Guinardia	1.458 ± 0.001	1.504 ± 0.004	1.34	1.371
n = 21	17.68 ± 3.89%	6.23 ± 1.23%	76.09 ± 4.52%	
Asterionellopsis	1.458 ± 0.001	1.504 ± 0.004	1.34	1.406
n = 15	34.87 ± 4.77%	15.45 ± 4.2%	49.68 ± 6.59%	
Prorocentrum	1.545 ± 0.031	1.504 ± 0.004	1.34	1.376
n = 23	14.37 ± 2.44%	3.76 ± 0.68%	81.87 ± 2.99%	
E. Huxleyi	1.577 ± 0.001	1.504 ± 0.004	1.34	1.546
n = 150	72.88 ± 2.37%	20.34 ± 1.63%	6.78 ± 0.26%	
Ciliate	1.381 ± 0.002	1.515 ± 0.006	1.34	1.427
n = 13	52.31 ± 3.76%	39.82 ± 2.69%	7.87 ± 0.83%	
Flocculate	1.352 ± 0.004	N/A	1.268 ± 0.013	1.2764
n = 10	~10%		~90%	

Measured volume portions of different phytoplankton structures as well as their respective RI values. The far right column shows the calculated bulk RI value for each different particle type. The last four entries are non-diatom particles, with the last entry being an inorganic particle, included as there is little to no literature available.

have different shapes and size distributions, as well as variability in the internal structure, there is some amount of uncertainty present in the measurements. The volume measurements show that a majority of diatoms have a cell wall that accounts for 20.5±10% of their total volume. The largest cell wall by percent volume was found with *Pseudo-Nitszchia,* measuring at 44.5±21.3%, likely due to the variation in size of the examined organisms (15-150 µm). Smaller organisms are expected to have a larger volume by percent accounted by the cell wall, while larger organisms display smaller percent volumes for their cell walls. In addition, the volumes of various structures vary between species (Desikachary and Dweltz 1961; Bernard 2009). The largest amount of

variation was found in the volume of chloroplasts, with different species ranging from 0 - 30%. In general, the chloroplast was the primary identifiable structure present in the measured marine organisms and accounted for 7.7±5.3% of the total volume of these organisms. The average water volume of marine phytoplankton in this study was 73.8±13.5%, which agrees well with previous measurements of 0.6 ± 0.2 by Aas (1996). The largest distinction in RI was attributed to the different membranes of phytoplankton.

Diatoms were found to have a bulk RI of 1.374 ± 0.019

which aligns with Aas's calculation of 1.38 ± 0.02. Similarly, the bulk value for *Prorocentrum spp.* of 1.376 ± 0.018 also lies within this range. Aas's calculated RI was for all phytoplankton types, not just diatoms. Coccolithophores, on the other hand, displayed a much higher bulk RI, 1.546 ± 0.035, as well as ciliates, 1.427 ± 0.03, compared to diatoms. These measurements show that using one bulk RI may not provide high enough resolution to distinguish different particle types within a marine sample. Table 2 shows the bulk RI values for particle groups, both absolute and relative to water. The RIs for most particles are all similar to each other, with coccolithophores and flocculates having the more extreme values due to their compositions: highly refringent calcite for coccolithophores, and a pocket of oil within the flocculate.

Table 2 *Bulk RI Values for Different Marine Particle Types*

Marine Particle Type	Bulk RI Value	Relative Bulk RI Value
Diatom	1.374 ± 0.019	1.026 ± 0.014
Prorocentrum spp.	1.377 ± 0.024	1.027 ± 0.018
E. Huxleyi	1.546 ± 0.035	1.154 ± 0.026
Ciliate	1.427 ± 0.03	1.065 ± 0.022
Flocculate	1.276 ± 0.013	0.953 ± 0.01

Listed bulk RI values for various marine phytoplankton and particles. The values are listed in both absolute (column 2) and relative to water (column 3).

CHAPTER IV Discussion

4.1 Comparison with previous results

The new method presented here allows, for the first time, a direct measurement of the RI of marine phytoplankton. The ability to measure these particles is an invaluable asset towards our complete understanding of the optical properties of particles in the oceans. Through the Nanolive 3D Cell Explorer, the RI of various structures of these particles was able to be measured, along with their volume calculations for different structures. Due to the limitations of the instrument itself, the values do need to be corrected. With both the RI and the volume of the different structures, a bulk RI for different particles was able to be calculated through the weighting of each structures' RI with its relative portion of the total volume. By determining this bulk RI, the particles can subsequently be better modeled as particles with this one bulk RI, with the assumption that the particles would behave as if it were homogenous.

Although little data is available, in examining previous studies, the data compares favorably. Table 3 lists available data for the four main organisms examined: diatoms, dinoflagellates, coccolithophores, and marine ciliates. The data compared against mine was gathered through various different means, such as phase microscopy or flow cytometric analysis. For diatoms, my values agree closely with the others available, however the values by both Poulin and Grant are higher. They both examined species which have a small size, *T. pseudonana* and *P. tricornatum*, both diatoms having an equivalent sphere diameter of less than 3.5 µm. The equivalent sphere diameter (ESD) is a way of comparing the relative sizes of different phytoplankton given that most are not spherical. For comparison, the two most abundant diatoms I examined were *Skeletonemia*

Table 3 *Comparisons of previously measured RI along with my calculated values*

Study	Particle	RI	Relative RI
This Study	Diatom	1.374 ± 0.019	1.026 ± 0.014
Aas 1996	Diatom	1.377 ± 0.004	1.0283 ± 0.0029
Poullin 2018	Diatom (*T. Pseudonana*)	1.4271	1.065
Poullin 2018	Diatom (*P. tricornutum*)	1.44318	1.077
McFarland 2020	Diatoms	1.3869	1.035
Grant 2020	Diatom (*T. pseudonana*)	1.411 ± 0.008	1.053 ± 0.006
This Study	Coccolithophore (*E. huxleyi*)	1.546 ± 0.035	1.154 ± 0.026
Aas 1996	Coccolithophore	1.381 ± 0.004	1.0313 ± 0.0029
Poullin 2018	Coccolithophore (*E. huxleyi*)	1.5209	1.135
Grant 2020	Coccolithophore (*E. huxleyi*)	1.461 ± 0.0067	1.091 ± 0.005
Terrats 2020	Coccolithophores	1.5142	1.13
This Study	Dinoflagellate (*Prorocentrum spp.*)	1.376 ± 0.024	1.027 ± 0.018
Aas 1996	Dinoflagellate	1.379 ± 0.004	1.0298 ± 0.0029
Nasiha 2015	Dinoflagellate	1.4-1.43	1.045-1.07
Maldondo 2008	Dinoflagellate	1.393-1.047	1.04-1.05
This Study	Ciliates	1.427 ± 0.03	1.065 ± 0.022
Morel 1991	Ciliates	1.399	1.044

RI values calculated for 4 different marine particle types: diatoms, coccolithophores, dinoflagellates, and ciliates along with previously published

spp. and *Chaetoceros spp.* both of which have a higher ESD. Table 4 shows the known equivalent sphere diameters available for the examined species. Poulin calculated the bulk RI of these particles through a coated sphere model, taking the two layers refractive indices and weighting them by layer thickness. With these smaller particles, the bulk RI is most affected by the value of the coating. This is because the coating represents the external membrane and, in most phytoplankton, this is a highly refringent material (silica or calcium carbonate). For the coccolithophores, the values I measured agree closely with previous measurements aside from Aas's. His measurements are consistently lower than

Table 4 *Equivalent Sphere Diameters of selected diatoms*

Source	Species	ESD (µm)
Yang et al. 2006	*Chaetoceros spp.*	4.27
Yang et al. 2006	*Skeletonemia spp.*	8.09
Yang et al. 2006	*P. tricornatum*	2.46
Kahl et al. 2008	*T. pseudonana*	3.5

Table 4 *Equivalent Sphere Diameters for 4 diatom species showing the difference in size of particles being examined*

all other measurements I could find. The intricate nature of these organisms through their internal and external structure is likely the culprit. He stated that internal structure was not considered past "a homogenous composition" throughout, whereas my measurements and the others collected utilized properties that could not ignore this feature (scattering and flow cytometry). With dinoflagellates, my values very strongly agree with previous results as well. Lastly, with ciliates, there was not much data available. The one study I found reported slightly lower values than I measured. However, this is likely due to the instrument missing the resolution in order to measure these tiny (<10μm) particles while capturing the intricate detail of the inner structure.

4.2 Application

In a 2011 paper, Zhang et al developed a method for determining the particle size distribution of a sample along with the RI of the different subpopulations within the sample (2011). The method takes a Volume Scattering Function and models it with small subpopulations with different particles of varying radii and RI in order to develop a reconstructed version of the measured VSF. The modeled subpopulations all model one portion of the overall VSF and when combined they accurately reconstruct the measured VSF in both shape and magnitude. This model result can be compared with a measured particle size distribution to see how well they compare as well. With an understanding of the RI distribution as well as a bulk RI for these various phytoplankton, we can incorporate these into the models and subsequently increase our accuracy in using them. Furthermore, we can use this knowledge as a way of verifying models. If we know the particle size distribution of a sample, and the refractive indices of the particles withing it, the VSF can be determined mathematically and compared with both the measured and

reconstructed VSFs from the model. With RI being one of the main contributing characteristics towards determining optical properties, increasing our understanding of these complex interactions is invaluable towards a complete understanding of the ocean itself. Many remote sensing satellites that are used for data collection rely on detecting backscatter signals and their interpretation. With different particles causing for distinctly different backscatter signals, being able to model the scatter caused by these particles, either in situ or in lab grown cultures, is invaluable, and relies in part on the bulk RI that has been developed.

With phytoplankton, there is great variability in the shape, size, structure, and composition between the many varied species in the oceans. Due to this, a complete and thorough understanding of these particles is necessary, however broad studies cannot hope to encompass it all. To further study these particles and their RI's, both structurally and in bulk, more studies need to be performed. Culturing these phytoplankton would offer the best way to study these particle characteristics. This would allow for culturing of the particles in conditions that prevent other particles from being present, allowing for concise measurement as well as examining the effects of just one particle type in instruments such as a LISST-VSF or Coulter Counter. This allows for these characteristics to be measured in a way that limits the amount of uncertainty. With a series of studies for various phytoplankton species, a concise understanding of the optical properties of phytoplankton would be possible.

4.3 Phytoplankton Geometry

For modeling these particles using Mie Theory, one of the main causes for uncertainty is the assumption that all particles are spherical (Mie 1908). Some single

phytoplankton cells are spherical in shape, like *E. Huxleyi*, but the majority are not, instead the shape of phytoplankton is usually described in terms of geometric shape (spherical, conical, ellipsoid, etc.) along with the shape elongation and flattening, resulting in over 50 different shapes being described for phytoplankton (Lifewatch Italy). A majority of the species I examined were box shaped and could not be approximated using a sphere. Furthermore, the variability in shapes between species is important as it shows that not all particles can be assumed to be the same shape. Diatoms are the most abundant phytoplankton in the oceans and they display an even more complex geometry in many cases. Many of these diatoms like to form colonial structures where they are all chained together, forming a larger structure with a higher level of geometry that can be described by a simple sphere. Furthermore, colony structures also vary between species, for instance, *Asterionellopsis spp*. colonies are shown to be formed of cells joined at their large valve face, with the pole extending out, with the overall colony spiraling out in a helical shape (Fig 9a). Conversely, *Skeletonemia spp.* colonies form by individual cells connecting end to end with a ring of protrusions giving an elongate rectangular shape to these colonies. (Fig 10d). Because of this, assuming these particles to be spherical does not truly encapsulate the shape of these particles.

4.4 Volume Fraction

Without an in depth understanding of the particle geometry, the modeling of these particles will have an amount of uncertainty due to the geometry itself. Ideally, we would have a different 3D Geometric shape constructed for each different phytoplankton, allowing us to accurately distribute the RI and accurately weight it across the whole organism. The modeling itself assumes the particles to be homogenous as well. This

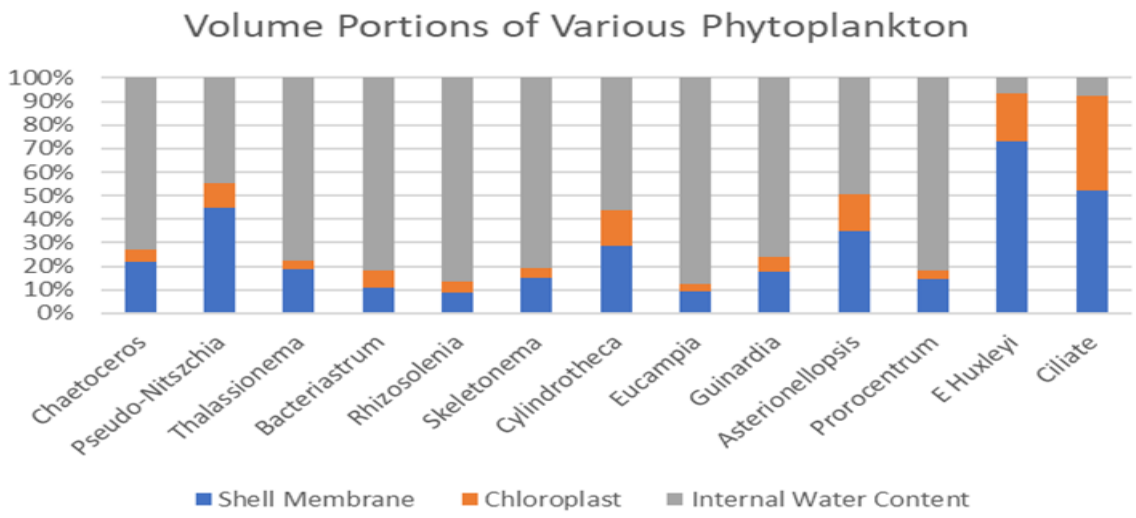

Figure 13 *Volume measurements for major portions (Chloroplast, Cell Membrane, and Water Content) for various measured phytoplankton particles during this study*

presents another issue that can only be partially solved. Not all organisms that belonged to the same species had the same measurements. In examining just diatoms, within species, there was a high amount of variation that was visible specifically with the chloroplast. Figure 13 displays the average values for the volumes of different particles measured. In examining the figure, high variation between different phytoplankton groups is clearly seen. In just examining diatoms, though their values may be similar, they do so clear variation between species. Furthermore, Table 5 shows the different species measured along with ranges for the percent volume occupied by their structures. In particular, the chloroplast occupied 5-10% of the species, however some species displayed much higher variance than the average. In examining the data for *Chaetoceros spp.* there were organisms with a chloroplast that was almost nonexistent, while others from the same sample displayed chloroplasts with volumes of close to 30% of the total. Furthermore, there is a large amount of variation present with the external membranes of these organisms. Some display low variation, however, there were some organisms with a

Table 5 *Range of volume portions of measured structures*

Species	Shell	Chloroplast	Water
Chaetoceros, n = 209	3.03-75.22%	0.17-30.57%	2.43-96.69%
Pseudo-Nitszchia, n = 53	11.08-75.46%	2.04-27.61%	6.16-86.7%
Thalassionema, n = 64	10.46-25.1%	1.16-7.35%	70.08-86.32%
Bacteriastrum, n = 15	6.38-16.77%	4.85-8.57%	78.38-85.05%
Rhizosolenia, n = 39	2.19-21.89%	0-33.12%	45.94-97.09%
Skeletonema, n = 296	7.19-25.37%	0.77-12.04%	63.87-91.82%
Cylindrotheca, n = 18	19.45-44.05%	10.76-20.7%	35.24-69.79%
Eucampia, n = 13	8.88-10.63%	2.58-3.27%	86.1-88.37%
Guinardia, n = 21	13.29-24.99%	4.59-7.98%	67.44-80.98%
Prorocentrum, n = 23	11.05-19.21%	2.64-5.19%	75.6-85.31%
E. Huxleyi, n = 150	52.6-84.9%	12.8-31.6%	1.9-8.9%
Cilliate, n = 13	42.6-61.8%	33.6-45.4%	3.8-9.7%

Calculated volume portions of the organisms measured in this study. Values are reported as the range of variation for each portion in terms of percent total volume.

membrane measuring 75% of their total volume, while others measured extremely volume percentages for their external membrane. Without a thorough understanding of the specific structural composition of different phytoplankton, both between and within singular species, the bulk RI will still have an amount of uncertainty associated with it due to these variations itself.

4.5 Ending Remarks

With an increased understanding of the optical properties of these particles, we are able to have a more complete understanding of the particles themselves. To do this, a more thorough understanding of the shape and internal structural variation of these particles is necessary. The RI is only one property that determines optical properties.

While it may be one of the more important properties, it demonstrates that a forward push needs to continuously be made towards a thorough understanding of these particles due to their ubiquity and vast number of uses applications towards scientific study. In considering optics specifically, as we understand more about these particles, we are able to better understand and deconvolute complex spectral signals into the contributions by single particle types. These spectral signals are utilized by numerous processes in order to serve as the primary way we monitor the Earth's surface both on a daily basis as well as over long time periods in order to study global trends. Ultimately our understanding of these particles will allow us to have a greater and more thorough comprehension of our oceans and the processes throughout.

CHAPTER V References

Aas, E. (1996). Refractive index of phytoplankton derived from its metabolite composition. *Journal of Plankton Research*, *18*(12), 2223–2249. https://doi.org/10.1093/plankt/18.12.2223

Ackleson, S. G., & Spinrad, R. W. (1988). Size and RI of individual marine particulates: a flow cytometric approach. *Applied Optics*, *27*(7), 1270. https://doi.org/10.1364/ao.27.001270

Ackleson, S. G., Spinrad, R. W., Yentsch, C. M., Brown, J., & Korjeff-Bellows, W. (1988). Phytoplankton optical properties: flow cytometric examinations of dilution-induced effects. *Applied Optics*, *27*(7), 1262. https://doi.org/10.1364/ao.27.001262

Bernard, Stewart et al. "Simulating the optical properties of phytoplankton cells using a two-layered spherical geometry." *Biogeosciences Discussions* 6 (2009): 1497-1563.

Bricaud, A., Bédhomme, A. louise, & Morel, A. (1988). Optical properties of diverse phytoplanktonic species: Experimental results and theoretical interpretation. *Journal of Plankton Research*, *10*(5), 851–873. https://doi.org/10.1093/plankt/10.5.851

Carder, K. L., Tomlinson, R. D., & Beardsley, G. F. (1972). A Technique for the Estimation of Indices of Refraction of Marine Phytoplankters. In *Limnology and Oceanography* (Vol. 17, Issue 6, pp. 833–839). https://doi.org/10.4319/lo.1972.17.6.0833

Charney, E., & Brackett, F. S. (1961). The spectral dependence of scattering from a spherical alga and its implications for the state of organization of the light-accepting pigments. *Archives of Biochemistry and Biophysics*, *92*(1), 1–12. https://doi.org/10.1016/0003-9861(61)90210-7

Desikachary, T. V., & Dweltz, N. E. (1961). *The chemical composition of the diatom frustule. Proceedings / Indian Academy of Sciences, 53(4), 157–165.* doi:10.1007/bf03051518

Faick, C. A., & Fonoroff, B. (1944). A precision apparatus for the rapid determination of indices of refraction and dispersion by immersion. *Journal of Research of the National Bureau of Standards*, *32*(2), 67. https://doi.org/10.6028/jres.032.020

Fan, H., Wu, W., Huang, Y., & Li, Z. (2017). RI inversion based on Mueller matrix method. *Selected Papers of the Chinese Society for Optical Engineering Conferences Held October and November 2016*, *10255*(November 2016), 102553N. https://doi.org/10.1117/12.2267696

Gerecht, A. C., Šupraha, L., Langer, G., & Henderiks, J. (2018). Phosphorus limitation and heat stress decrease calcification in Emiliania huxleyi. *Biogeosciences*, *15*(3), 833–845. https://doi.org/10.5194/bg-15-833-2018

Grant, Stephen & Richford, Kyle & Burdett, Heidi & McKee, David & Patton, Brian. (2020). Low-cost, open-access quantitative phase imaging of algal cells using the transport of intensity equation. Royal Society Open Science. 7. 191921. 10.1098/rsos.191921.

Green, R. E., Sosik, H. M., Olson, R. J., & DuRand, M. D. (2003). Flow cytometric determination of size and complex RI for marine particles: comparison with independent and bulk estimates. *Applied Optics*, *42*(3), 526. https://doi.org/10.1364/ao.42.000526

Guillard, R. R. L., & Ryther, J. H. (1962). Studies of Marine Planktonic Diatoms: Cyclotella nana hustedt and Detonula confervacea (CLEVE) . *Can. J. Microbiol.*, *8*(1140), 229–239.

Haunost, M., Riebesell, U., D'Amore, F., Kelting, O., & Bach, L. T. (2021). Influence of the Calcium Carbonate Shell of Coccolithophores on Ingestion and Growth of a Dinoflagellate Predator. *Frontiers in Marine Science*, *8*(June), 1–13. https://doi.org/10.3389/fmars.2021.664269

Kahn, Norman Swift, Elijah, (1978), Positive buoyancy through ionic control in the nonmotile marine dinoflagellate *Pyrocystis noctiluca* Murray ex Schuett, *Limnology and Oceanography*, 23, doi: 10.4319/lo.1978.23.4.0649.

Kahl, L. & Vardi, Assaf & Schofield, Oscar. (2008). Effects of phytoplankton physiology on export flux. Marine Ecology-progress Series - MAR ECOL-PROGR SER. 354. 3-19. 10.3354/meps07333.

Maldonado, D. J. C. (2008) "Spectral Properties and Population Dynamics of the Harmful Dinoflagellate *Cochlodinium polykrikoides* (Margalef) in Southwestern Puerto Rico," Ph.D. dissertation, Dept. Marine Sciences, Univ. Puerto Rico, Mayagüez, P.R.

McFarland, M., Nayak, A. R., Stockley, N., Twardowski, M., & Sullivan, J. (2020). *Enhanced Light Absorption by Horizontally Oriented Diatom Colonies. Frontiers in Marine Science, 7.* doi:10.3389/fmars.2020.00494

Mathews, I. M. (1914). *RI and density. Journal of the Franklin Institute, 177(6), 673–686.* doi:10.1016/s0016-0032(14)90992-9

Morel, A., & Ahn, Y.-H. (1991). *Optics of heterotrophic nanoflagellates and ciliates: A tentative assessment of their scattering role in oceanic waters compared to those of*

bacterial and algal cells. Journal of Marine Research, 49(1), 177–202. doi:10.1357/002224091784968639

Mie, G. (1908), Beiträge zur Optik trüber Medien, speziell kolloidaler Metallösungen. Ann. Phys., 330: 377-445. https://doi.org/10.1002/andp.19083300302

Nam, O., Suzuki, I., Shiraiwa, Y., & Jin, E. (2020). Association of Phosphatidylinositol-Specific phospholipase C with Calcium-Induced Biomineralization in the Coccolithophore Emiliania huxleyi. *Microorganisms*, *8*(9), 1–17. https://doi.org/10.3390/microorganisms8091389

Nasiha, H. J., & Shanmugam, P. (2015). *Estimating the Bulk RI and Related Particulate Properties of Natural Waters from Remote-Sensing Data. IEEE Journal of Selected Topics in Applied Earth Observations and Remote Sensing, 8(11), 5324–5335.* doi:10.1109/jstars.2015.2439581

Organelli, E., Dall'Olmo, G., Brewin, R. J. W., Tarran, G. A., Boss, E., & Bricaud, A. (2018). The open-ocean missing backscattering is in the structural complexity of particles. *Nature Communications*, *9*(1). https://doi.org/10.1038/s41467-018-07814-6

Pollaro, L., Dalla Piazza, B., & Cotte, Y. (2015). Digital Staining: Microscopy of Live Cells Without Invasive Chemicals. *Microscopy Today*, *23*(4), 12–17. https://doi.org/10.1017/s1551929515000590

Poulin, C., Zhang, X., Yang, P., & Huot, Y. (2018). Diel variations of the attenuation, backscattering and absorption coefficients of four phytoplankton species and comparison with spherical, coated spherical and hexahedral particle optical models. *Journal of Quantitative Spectroscopy and Radiative Transfer*, *217*, 288–304. https://doi.org/10.1016/j.jqsrt.2018.05.035

Poulin, C., Yang, P., & Huot, Y. (2018). "Diurnal variations of the optical properties of phytoplankton in a laboratory experiment and their implication for using inherent optical properties to measure biomass," Opt. Express 26, 711-729 (2018)

Rost, B., & Riebesell, U. (2004). *Coccolithophores and the biological pump: responses to environmental changes. Coccolithophores, 99–125.* doi:10.1007/978-3-662-06278-4_5

Santomauro, G., Sun, W. L., Brümmer, F., & Bill, J. (2016). Incorporation of Zinc into the Coccoliths of the Microalga *Emiliania huxleyi*. *BioMetals*, *29*(2), 225–234. https://doi.org/10.1007/s10534-015-9908-y

"Shape List for Phytoplankton." *Phytoplankton Virtual Research Environment*, Lifewatch Italy, https://www.phytovre.lifewatchitaly.eu/vre/shapes-list/?filter=COMPLETE_LIST.

Spinrad, R. W., & Brown, J. F. (1986). Relative real RI of marine microorganisms: a technique for flow cytometric estimation. *Applied Optics*, *25*(12), 1930. https://doi.org/10.1364/ao.25.001930

Terrats, L., Claustre, H., Cornec, M., Mangin, A., & Neukermans, G. (2020). *Detection of coccolithophore blooms with BioGeoChemical-Argo floats. Geophysical Research Letters.* doi:10.1029/2020gl090559

Twardowski, M. S., Boss, E., Macdonald, J. B., Pegau, W. S., Barnard, A. H., & Zaneveld, J. R. V. (2001). *A model for estimating bulk RI from the optical backscattering ratio and the implications for understanding particle composition in case I and case II waters. Journal of Geophysical Research: Oceans*, *106(C7)*, *14129–14142.* doi:10.1029/2000jc000404

Walker, C. E., Heath, S., Salmon, D. L., Smirnoff, N., Langer, G., Taylor, A. R., Brownlee, C., & Wheeler, G. L. (2018). An Extracellular Polysaccharide-Rich Organic Layer Contributes to Organization of the Coccosphere in Coccolithophores. *Frontiers in Marine Science*, *5*(AUG), 1–12. https://doi.org/10.3389/fmars.2018.00306

Yang, R.-J., Wang, X.-L., Zhang, Y.-Y., & Zhan, Y.-J. (2006). *Influence of cell equivalent spherical diameter on the growth rate and cell density of marine phytoplankton. Journal of Experimental Marine Biology and Ecology*, *331(1)*, *33–40.* doi:10.1016/j.jembe.2005.09.015

Zaneveld , J. Ronald V., Roach, David M., H. P. (1974). The determination of the index of refraction distribution of oceanic particles. *Journal of Geophysical Research: Oceans*, *79*(27), 4091–4095. https://doi.org/doi:10.1029/jc079i027p04091

Zhang, X., Twardowski, M., & Lewis, M. (2011). Retrieving composition and sizes of oceanic particle subpopulations from the volume scattering function. *Applied Optics*, *50*(9), 1240–1259. https://doi.org/10.1364/AO.50.001240

Zernike, F. (1942). Observation of Transparent Objects. *Physica*, *10*, 974–986.